Surface acoustic wave-induced precise particle manipulation in a trapezoidal glass microfluidic channel

2012 J. Micromech. Microeng. 22 025018

(http://iopscience.iop.org/0960-1317/22/2/025018)

J. Micromech. Microeng. **22** (2012) 025018 (11pp) doi:10.1088/0960-1317/22/2/025018

Surface acoustic wave-induced precise particle manipulation in a trapezoidal glass microfluidic channel

L Johansson[1,2], J Enlund[2], S Johansson[2], I Katardjiev[2], M Wiklund[1] and V Yantchev[2]

[1] Department of Applied Physics, Albanova/KTH, Roslagsv. 30B, SE-114 19, Stockholm, Sweden
[2] Department of Engineering Sciences, Ångström Laboratory, Uppsala University, PO Box 534, SE-751 21, Sweden

E-mail: linda.johansson@biox.kth.se

Received 1 November 2011
Published 25 January 2012
Online at stacks.iop.org/JMM/22/025018

Abstract

Surface acoustic wave (SAW) excitation of an acoustic field in a trapezoidal glass microfluidic channel for particle manipulation in continuous flow has been demonstrated. A unidirectional interdigital transducer (IDT) on a Y-cut Z-propagation lithium niobate ($LiNbO_3$) substrate was used to excite a surface acoustic wave at approximately 35 MHz. An SU8 layer was used for adhesive bonding of the superstrate glass layer and the substrate piezoelectric layer. This work extends the use of SAWs for acoustic manipulation to also include glass channels in addition to prior work with mainly poly-di-methyl-siloxane channels. Efficient alignment of 1.9 μm polystyrene particles to narrow nodal regions was successfully demonstrated. In addition, particle alignment with only one IDT active was realized. A finite element method simulation was used to visualize the acoustic field generated in the channel and the possibility of 2D alignment into small nodal regions was demonstrated.

(Some figures in this article are in colour only in the electronic version)

1. Introduction

Acoustic manipulation of particles and cells by acoustic radiation forces has been exploited by bulk acoustic wave (BAW) excitation in microfluidic channels [1–6] and in droplets [7] in the range of 1–10 MHz. Applications of acoustic manipulation by radiation forces in channels for continuous flow are for instance trapping of cells [8] for cell assays [9], enrichment of one cell type from a medium [10], enrichment of molecules binding to a bead surface [11], cleaning of media by the removal of one cell type [12], free flow acoustophoresis into multiple outputs [13], micro-fluorescence-activated cell sorters (FACS) [14], micromixers [15] and alignment in flow cytometry [16–18]. Recently, the driving frequency was extended to 40 MHz range by the use of interdigital transducers (IDTs) to excite a surface acoustic wave (SAW) that generates an acoustic field in a superstrate poly-di-methyl-siloxane (PDMS) channel [18–20]. Generally SAW transducers have been used in microfluidics for droplet manipulation in open planar fluidics to excite different acoustic effects at increasing input power [21], such as droplet mixing [22] and particle gathering by acoustic streaming [23], droplet transportation on a hydrophobic surface [22, 24], droplet ejection [25] and droplet atomization [26]. Additionally, particle gathering in a droplet by acoustic radiation force has been demonstrated for SAW transducers [27]. In closed channels, SAW-induced manipulation has been demonstrated for acoustic mixing [28, 29], for pumping [30], for filling fluid into the channels [31] and for drop manipulation [32] in addition to the above-mentioned particle manipulation by acoustic radiation forces [18–20, 33, 34].

Here we present for the first time SAW-excited particle manipulation in a superstrate glass channel. A first motivation regards manufacturing and integration. This work evaluates if it is possible to extend the use of SAWs for acoustic manipulation in PDMS and the more exclusive material and design used for the Stoneley wave [34] and the fabrication method for laser structuring in the piezoelectric substrate [33]

to also include the microfluidic commonly used glass material [35]. While the PDMS material is ideal for fast prototyping and bonding to silicon-based materials, the hydrophobic surface properties of native PDMS and the hydrophobic recovery of the PDMS surface may cause clogging due to particles sticking to the surface and high fluidic resistance when filling the channel with water. Other issues are sample loss by absorption into the PDMS material, change of the sample environment due to the release of uncured monomers from the polymer [36] and solvent swelling. Hence, physical and chemical modifications are commonly employed such as plasma oxidation, chemical surface modifications [37], bulk additives [38, 39], extraction of the uncured monomers by solvent swelling of the polymer [40] and 48 h heat treatment [41]. Additionally, the choice of superstrate material is of interest also from the perspective of integration with other operations such as detection. A second motivation regards the properties of the acoustic field in the channel. Similar to the state-of-the-art technology with high acoustic impedance channel BAW transducer particle manipulation devices [1–6], where rectangular or close to rectangular cross-section and half-wavelength width channels are commonly employed, the channel used here is expected to enable a strong resonance in the fluidic layer. This property is not expected for the mechanically flexible PDMS with a small mismatch in acoustic impedance relative water. In this work, we evaluate the significance on the acoustic field of the channel geometry and size for the case of high-impedance superstrate channel material. Specifically, a trapezoidal channel geometry and channel width of approximately half wavelength of the surface acoustic wave of the substrate was used. The position of the alignment nodes relative to the channel walls, the inter-node distances and the shape and size of the nodal area determine how the device can be used for particle alignment to certain positions in the channel. Control of the acoustic node positions is strongly related to factors such as system reproducibility and fabrication alignment tolerances. In previous work with SAW-transducer systems and PDMS channel [18] or without side-walls [42], the inter-node distance has been generally reported to be $\lambda_{SAW}/2$. Regarding the size of the nodal region, it is expected that the use of higher frequency can be employed to align smaller particles to a narrower nodal region. Small nodal regions enable more precise alignment, which in sensor applications can offer system benefits such as sensitive, single-cell, high speed detection of small particles and in lower concentration samples. Moreover, it is of interest if the device can be used without sheath flow operation and if the alignment can also be obtained in the vertical direction. In this work, we evaluate by finite element method (FEM) simulation if a non-plane-parallel channel cross section, such as hemispherical [34] or a trapezoidal which are obtained by isotropic etching, can be used to generate particle alignment also in the vertical direction for the case of high impedance mismatch at the fluid–channel interface.

Precise particle alignment by acoustic forces to narrow nodal regions in continuous flow has been targeted in fewer studies than high concentration sample manipulation. Precise alignment has been demonstrated for 10 μm diameter particles at maximum 10 MHz [43–45] and can also be found for 0.5 μm diameter by Stoneley wave at 40 MHz [34]. Moreover, 2D precise alignment to one or several points in the channel cross-section plane by simultaneous horizontal and vertical for continuous flow is not commonly performed. Most commonly in continuous flow particle manipulation devices, the particles are aligned to a vertical nodal plane region positioned in the middle of the fluid [2, 3, 46, 47] or at one of the channel walls [47–52] in a rectangular or slightly tapered rectangular channel geometry at a maximum of 5 MHz. Precise alignment to small detection points enable single-cell detection applications. Since 2D alignment ensures that all particles in a parabolic flow profile travel at the same speed, they can be detected as single events without overlap. Applications are found in alignment prior to sensor detection for sheathless operation in parabolic flow profiles. In the case of flourescent detection, the need for a scanning laser setup to evaluate signals from the entire channel volume is omitted. If multiple sensors are used, multiple alignment positions and larger volumetric flow rate can be employed. Alignment to a surface is desired for the detection by sensors positioned at the channel wall, for instance an optical evanescent field sensor. These applications have been targeted by acoustic manipulation for batch mode operation to a larger sensor surfaces by different device designs [47–52]. Alignment to a small point on a surface in combination with a small area sensor can be used in continuous operation and single particle detection. For the case of alignment to a single point, additional applications exist such as pre-alignment in fluorescent-activated cell sorter (FACS) and prior to sheathless acoustic particle manipulation operations in parabolic flow such as field flow fractionation.

The difficulty with simultaneous vertical and horizontal 2D alignment by acoustic radiation forces is at least partly related to the effect of coupling of harmonic oscillators leading to more complicated resonance patterns at the coinciding resonance frequency. 2D resonance mode coupling in a fluidic cavity has been studied analytically by observing the resonance pattern of two orthogonal ideal standing waves [7], where the coupled oscillation term was shown to dominate if the same frequency is used in the two directions. However, by the use of two different frequencies matched to the channel width and height, respectively, vertical and horizontal 2D alignment to a point has been demonstrated for 10 μm diameter particles by BAW transducers [43–45]. Additionally, in a preliminary study, vertical and horizontal alignment was described to be performed by matching the channel width and height close to an overtone and the fundamental frequency, respectively, however requiring a large sheath flow [53]. In principle, particle alignment by tubular transducers in circular cross-section capillary channels is expected to generate 2D horizontal and vertical alignment, which has been demonstrated for a multinode case [54]. In a PDMS channel, vertical alignment has been demonstrated [55]. Related work is the use of a hemispherical reflector to generate alignment in the two horizontal directions in a 96-well plate [56]. To the authors knowledge, simultaneous horizontal and vertical 2D alignments have not been performed by a non-plane-parallel channel cross section in a microstructured channel. Nor has

2D horizontal and vertical alignment been demonstrated in microstructured glass channels by operating at one single frequency without a large sheath flow.

2. Theory and principles

For a standing wave in the fluidic channel with a sinusoidal pressure distribution along the axis of propagation, z, the primary acoustic radiation force, F_{Prim}, can be described by [57]

$$F_{\mathrm{Prim}} = \frac{V P_0 \pi}{2\rho_0 c_0^3} f \Theta \sin\left(2\pi \frac{z}{\lambda/2}\right), \quad (1)$$

where V is the volume of the particle, f is the driving frequency, P_0 is the amplitude of the acoustic pressure oscillations, ρ_0 is the density in the absence of sound, c_0 is the sound velocity of the medium, λ is the wavelength and θ is the acoustic contrast factor:

$$\Theta = \frac{5\rho - 2\rho_0}{2\rho + \rho_0} - \frac{\beta}{\beta_0}, \quad (2)$$

where $\beta = 1/(\rho c^2)$ is the compressibility of the fluid and β_0 is the compressibility of the particle. Compressible spherical particles are assumed, no acoustic scattering effects from walls are accounted for and the expression is valid under the requirement that particles are small relative the wavelength. For particles or cells with a positive acoustic contrast factor, the radiation force is directed toward a pressure node and for the case of negative contrast factor toward a pressure anti-node. To generate particle motion of a particle in a fluid, the acoustic radiation forces have to be large enough to overcome Stokes drag force. While the radiation force determines the strength of the acoustic manipulation effect, the acoustic radiation force potential field, U, where $F = -\mathrm{d}U/\mathrm{d}x$, displays the positions at which the particles will be gathered. The particles with positive acoustic contrast factor will be aligned to a pressure node according to theory.

Particle manipulation by SAW is envisioned to generate many advantageous properties. Compared with the $PbZr_{1-x}Ti_xO_3$ (PZT) piezoelectric material usually employed for BAW excitation, the lithium niobate employed here for SAW excitation is associated with low losses in the single crystalline piezoelectric material [58]. Hence, low temperature increase from material losses are expected in the fluid at the power levels employed. Viscous losses in the fluid increases with increasing frequency since the absorption coefficient is proportional to the frequency squared. The viscous absorption in a water layer of 100 μm is less than 0.1% at 10 MHz and though several times larger at 40 MHz still less than 1% [59]. The IDT enables a planar design and easy inspection by being positioned outside the channel region. Furthermore, a higher driving frequency than is usually employed for acoustic particle manipulation enables stronger acoustic forces for a certain acoustic pressure. High forces for instance enable manipulating particles with lower acoustic contrast factor relative to the medium. The acoustic power level in the fluid layer depends on a number of factors: the response of the piezoelectric material, the quality factor of the transducer design which amplifies the response, the electrical matching with the function generator, the energy coupling into the fluidic channel, resonance in the channel structure, etc. For the device presented here, a reflector structure outside the IDTs ensures directivity of the transducers that approximately doubles the energy into the fluid relative to a non-directional transducer.

From an acoustic perspective, glass has fundamentally different material properties than PDMS which will influence the appearance of the acoustic field in the fluid. Glass has significantly higher acoustic impedance and lower viscous losses. The path to transport energy into the fluid, the magnitude of energy and the resonance build-up in superstrate and in the fluid layer are factors that influence the appearance and the magnitude of the acoustic field in the fluid layer and the ability to perform efficient particle manipulation. The excitation of a fluid layer in a PDMS superstrate has been explained by excitation from the piezoelectric channel bottom by a standing surface acoustic wave (SSAW) in the substrate that is generated by two counter-propagating waves [18]. The authors expect that when the traveling SAW encounters a glass/$LiNbO_3$-interface or a PDMS/$LiNbO_3$-interface energy will be transmitted into the glass/PDMS bulk. Thus, a certain fraction of the traveling wave will be diffracted into the bulk at some angle and as the wave propagates, more and more of the energy present at the surface will couple into the bulk. Material losses of the PDMS material (Elastosil RT 601) in the range 4–14 MHz display a high attenuation coefficient for the longitudinal wave, $\alpha = 6.06^{0.49}$ [60]. Assuming this relation is valid also at 40 MHz, longitudinal losses are in the range of 400 m^{-1} and the pressure amplitude decreases by approximately 50% in 1.5 mm. In a glass superstrate, on the other hand, the viscous absorption loss is considerably lower and the acoustic energy can propagate inside the glass and resonances can build up by reflections at the superstrate–air interfaces and inside the fluid cavity. For the case evaluated here, it is expected that especially the appearance of the acoustic field along the bonding region and around the cavity can influence the acoustic field in the fluidic layer.

3. Experimental details

3.1. Device design

The principal setup of the IDT on the Y-cut Z-propagating lithium niobate ($LiNbO_3$) substrate is shown in figure 1. The IDT electrodes are organized into 40 groups of one wavelength with three strips in each pair having potentials (++−), which makes them non-reflecting and therefore no energy is trapped underneath the electrode structure. The spacing and width of the electrodes are $\lambda/6$ (16 μm). The frequency of operation is determined by the sound velocity of a surface acoustic wave divided by the wavelength defined by the electrode period (96 μm). A reflector structure of 20 electrode strips with width and spacing of $\lambda/4$ (24 μm) is positioned on the outer side of each transducer and enables a certain degree of unidirectionality of the radiated acoustic wave. The two IDTs with their respective reflectors have an aperture of 9 mm and are placed symmetrically at a distance of approximately

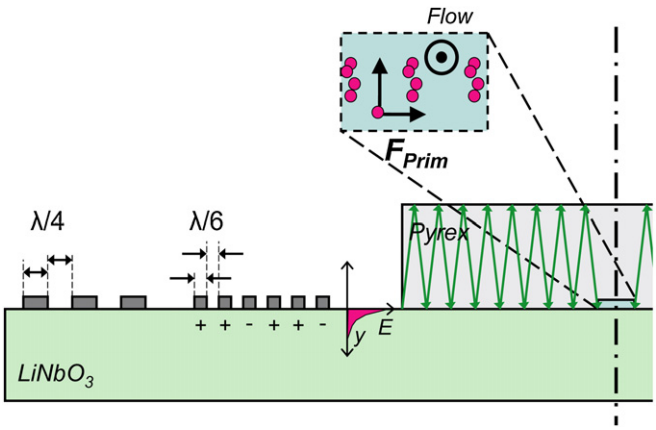

Figure 1. Cross-section of the device showing the reflector strips ($\lambda/4$ spacing and width), the IDT strips ($\lambda/6$ spacing and width) (with the applied electric potential) on the piezoelectric substrate and the glass superstrate where the acoustic forces cause alignment of the particles in the fluidic layer. The schematic energy distribution E, of the surface acoustic wave outside the channel structure is shown as well as wave propagation inside the Pyrex glass (arrows). The fluid flow direction is shown as well as the primary radiation force, F_{Prim} and the resulting alignment of particles.

5 mm from the channel centerline on the piezoelectric substrate. The glass channel is positioned manually with an estimated accuracy less than 1 mm. A photo of the device is shown in figure 2(*A*).

An acoustic standing wave, which is required for the acoustic radiation force in equation (1), is formed by interference of two counter-propagating waves emitted by the IDTs. For a driving frequency in the range of 30 MHz, the wavelength in water is around 40 μm. In this work the evaluated channel width (at the channel bottom) was 60 μm. At 35 MHz, the 500 μm distance of the glass layer at either side of the channel corresponds to approximately 60 λ. Hence, overtones for the distance along the superstrate interface are positioned 0.6 MHz apart.

3.2. Device fabrication

The use of a glass channel on a SAW substrate requires bonding of two stiff materials, with high and different temperature coefficients. Here the cavity sealing was performed by a thin adhesive layer of SU8 as employed in MEMS-packaging [61] but not generally employed in microfluidics. The adhesive bonding method was selected since it is not sensitive to the surface roughness expected for a wet etched borosilicate glass and does not require precise matching of the thermal expansion coefficients of the two layers.

3.2.1. $LiNbO_3$ transducers. A 300 μm thick 100 mm SAW grade Y-cut $LiNbO_3$ wafer was used in the *Z*-propagation direction. The process flow is shown in figure 3. The lift-off step was initiated by cleaning the wafer in (1:1 H_2SO_4:H_2O_2) for 30 min, followed by standard lithography (1 μm, Shipley 1813 photoresist) to define the IDT pattern and finally metallization by e-beam evaporation (80 nm/10 nm Au/Ti, 10^{-5} mbar). Prior to evaporation, oxygen plasma treatment (75 W, 5 min) was performed to remove residual resist from the patterned grooves in the resist and to improve metal adhesion. After metal deposition, the wafers were immersed in acetone with ultrasound to remove the excess metal and photoresist. The wafers were then rinsed in isopropanol and dried in N_2 before being cut with a dicing saw. A close-up of the IDT can be seen in figure 2(*B*).

3.2.2. Borosilicate processing. The 700 μm borosilicate wafers (Emmaboda Glasteknik, Sweden) were wet-etched in a 10:1 HF (49%):HCl (37%) solution with a lithographically defined mask of e-beam-evaporated Au/Ti (500 nm/10 nm) and photoresist (10 μm AZ4562, Clariant). The HCl improves the surface roughness of the etched surfaces by transforming the insoluble products, such as CaF_2, MgF_2 and AlF_3, into soluble ones [62]. The high HF concentration enabled a fast borosilicate etch rate of 8.5 μm min^{-1}. The borosilicate wafers were cleaned in (1:1 H_2SO_4:H_2O_2) for 30 min, RCA1 (2:2:1 H_2O: H_2O_2: NH_4OH) and RCA2 (1:1:6 H_2O_2:HCl:H_2O) prior

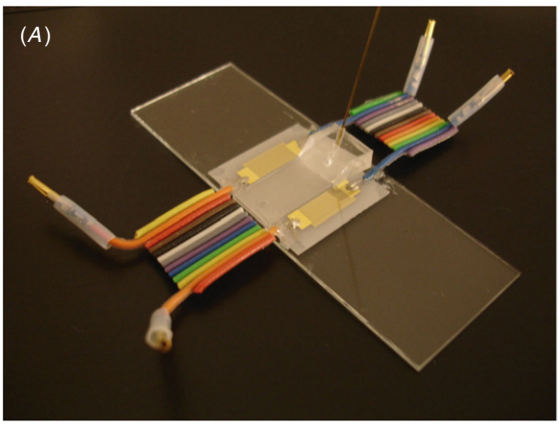

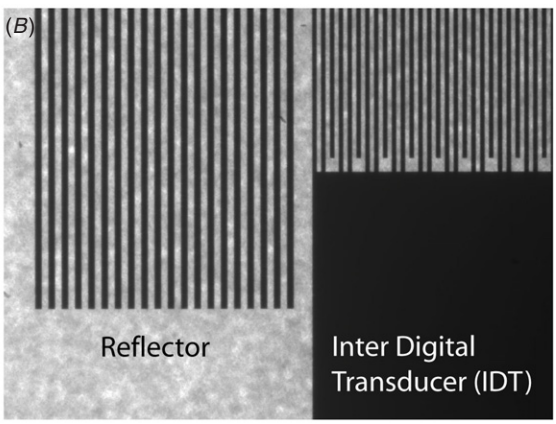

Figure 2. (*A*) The system setup with the two IDT structures on the single-polished (frosty) lithium niobate substrate and glass superstrate mounted on a microscope glass slide. Fluidic connection is provided by an inlet glass capillary and a PDMS seal. The device is electrically connected for single IDT excitation or dual excitation of the two IDTs in series. (*B*) Close-up of the IDT strips and the reflector strips.

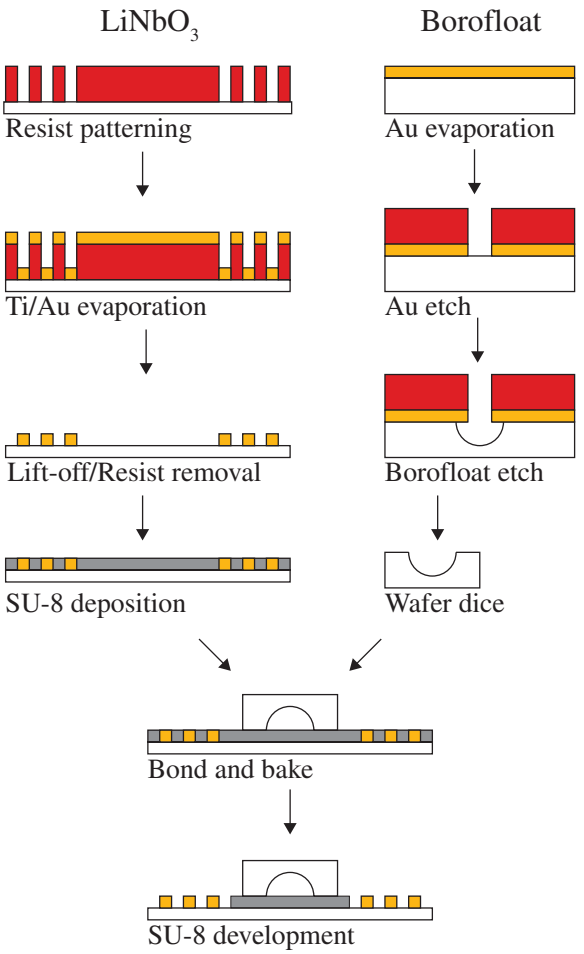

Figure 3. Device fabrication. Left: lift-off Au patterning of the $LiNbO_3$ with Ti as the adhesion layer. Right: wet etch of borosilicate glass by HF:HCl with a Au and photoresist mask layer to form a non-plane-parallel channel cross-section, here illustrated by a hemispherical cross-section. Bottom: adhesive chip-level bonding by SU-8.

to evaporation. The evaporation was performed in steps of 100 nm at a time with a 20 min wait period in between depositions to minimize the occurrence of pinholes in the Au mask. The Au mask was etched in KI solution ($KI:I_2:H_2O$ 4:1:40, v/v). Three minutes etching of the borosilicate wafers with mild stirring resulted in a 25 μm deep and 60 μm wide channel. A thick tape was used to cover the glass wafer backside during the etch process. The Au mask layer was subsequently removed by the KI-solution. Inlet holes were drilled by a 1 mm diamond-tipped drill and the wafers diced with a dicing saw. Before and after drilling, the etched glass structure was heated to the softening temperature of 560 °C and slowly cooled down in order to reduce any induced stress due to etching and drilling. The etch profile of the channel is shown in figure 4. The profile has tapered walls rather than a hemispherical profile which is a phenomenon observed in the literature for faster etching [63] and hence was a result of the selected etch recipe and a desire to avoid pin holes in the etch mask. While a geometry such as a circular or a rectangular shape would be preferred over the tapered walls for supporting an ideal standing wave, in a practical case when

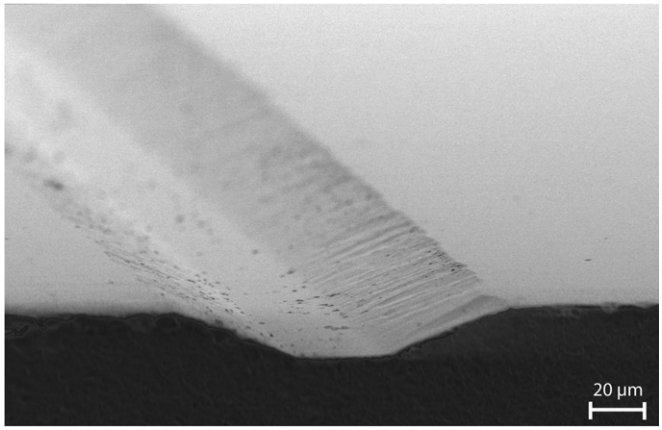

Figure 4. SEM image of channel cross-section displaying the tapered channel profile and ridges in the channel walls.

exciting a glass channel with an external transducer, it was found that walls with tapered slope and ridges (similar as employed here) enabled equally good acoustic manipulation as a perfectly rectangular profile [46].

3.2.3. SU-8 bonding. Bonding of the borosilicate glass and lithium niobate substrate was performed on chip-level by an adhesive SU8-5 layer (MicroChem). Bonding with SU-8 has previously been used e.g. for bonding of lithium niobate to silicon at 60 °C, at a pressure of 500 N in vacuum for 1 h in a wafer bonding machine [64, 65]. The $LiNbO_3$ chip and the glass chip were heated (200 °C, 5 min) to dehydrate the surface and promote adhesion. A 4 μm SU-8 layer was spun on to the $LiNbO_3$ (4000 rpm, 30 s) and were left to rest for 30 min on a flat surface to reduce the height of the edge bead and allow for some drying of the SU-8. The channel structure was aligned manually and a light pressure was applied by pressing a pair of tweezers onto the surface thereby forming an initial bond at room temperature. To soften the SU-8 and promote a void-free bond, the chip was heated on a hot plate (65 °C, 5 min) while applying pressure with tweezers. After forming the bond, the SU-8 was illuminated through a chromium on glass mask to further cross-link the adhesive. After the exposure, the excess SU-8 covering the IDTs was removed by the SU-8 developer (mrDev 600, MicroChem) and isopropanol. Last, a 5 min post-exposure bake at 65 °C was performed to further strengthen the adhesive bond.

3.2.4. Fluidic and electric connections. Fluidic connections were provided by bonding a PDMS part to the glass and inserting a polyethylene tubing of 380 μm inner diameter (Intramedic BD, Becton Dickinson) outside a glass capillary (outer diameter 365 μm and inner diameter 95 μm). Electrical connections were provided by conductive epoxy (Circuitworks, Chemtronics) covered by epoxy (Plastic Padding) for mechanical robustness. The device was glued onto a glass slide for fitting into the microscope holder.

3.3. Set-up and quantification

The transducers were excited by a high-frequency function generator (Hewlett-Packard 8116A Pulse/Function generator) with a maximum power output of 320 mW or 16 V_{pp} for a 50 Ω load. The minimal step size of this device was 0.1 MHz. An Agilent 4395A Network Analyzer was used for impedance measurements (0.22 V at 50 Ω). For this proof-of-principle evaluation, a straight channel with one inlet and one outlet was used. The ability to manipulate particles was evaluated by observing the particle alignment by an inverted Nikon TE-2000-U fluorescence microscope (Hg-lamp excitation) with a high sensitive cooled CCD camera (Spot Diagnostic Instruments). Initially the channels were filled with ethanol since its fluid resistance is lower than that for water. A syringe pump (Univentor 864) was used with a 100 mL Hamilton syringe. Green fluorescing 1.9 μm polystyrene beads (Polymer Microspheres, Duke Scientific Corp.) of 1.05 g cm^{-3} density in de-ionized water with 0.5% (v/v) Tween (to prevent particle agglomeration) were used. Measurements were performed for a single IDT and for the two IDTs in series. By connecting the electrodes on both sides of the device, the transducers were operated in series, dividing the supplied voltage. The flow velocity was in the range of 0.01 μL min^{-1} (8 mm s^{-1}) where the uncertainty is related to flow variations due to some reduction of channel width at some places along the channel where SU-8 had leaked into the channel.

3.4. FEM modeling of acoustic fields

FEM simulations (Comsol Multiphysics 4.1) were performed to visualize the acoustic radiation force potential field in the fluid layer and parameters that influence it. The device cross-section was modeled in 2D in a frequency analysis. A simplified IDT-electrode geometry of four periods of electrode stripes were used, with alternating potential and ground (+ − +−) positioned on either side of the glass structure and excited by a sinusoidal potential of 10 V. For simplicity, only a few wavelengths of the glass solid was modeled inside an outer layer of glass with high acoustic absorption. An isotropic loss factor of 0.9 was introduced in the outer glass layers, which were surrounded by an air layer. The choice of geometry with an outer absorbing layer has the consequence of reducing but not eliminating the influences of reflections and resonance build up inside the glass structure so the analysis is limited to this case. The height of the inner glass layer is approximately one wavelength and the width is approximately 2.25 wavelengths of the glass material. As a consequence of the manual alignment method, it is expected that the SAW node position in the substrate relative to the channel walls will differ between devices, since the acoustic path length depends on the exact position of the glass channel. In general, since not all geometric parameters are exactly as in the device, a perfect agreement between simulation and measurements is not expected but rather to be able to study typical appearances and trends. Material properties for the glass was Young's modulus of 63 GPa and Poisson's ratio of 0.20 and for SU8 Young's modulus of 4.2 GPa and Poisson's ratio of 0.22.

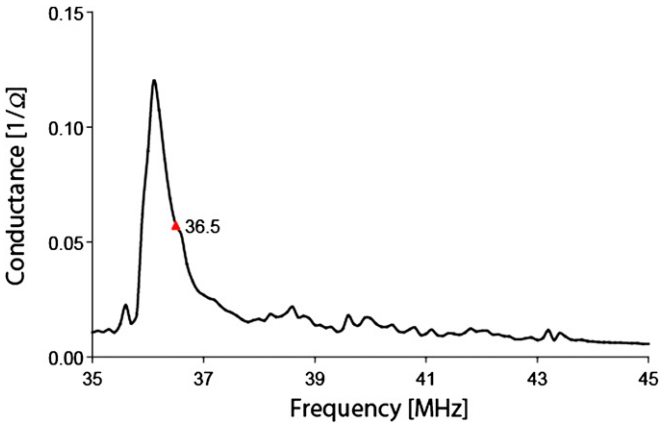

Figure 5. Conductance spectra for the lithium niobate single IDT operation. Particle alignment was demonstrated at 36.5 MHz.

4. Results and discussion

4.1. Impedance measurements

The conductance spectra of the single IDT is shown in figure 5. The main resonance peak is found at 36.1 MHz where the maximum acoustic output from the transducer is obtained. The operation with 40 groups (120 strips) of electrodes generates a bandwidth in the range of 1 MHz as is observed for the main peak in the graph. The broadband IDT has a quality factor Q in the range of 20. Indicated in the figure is the frequency where particle alignment was obtained in the device at 36.5 MHz.

4.2. Particle alignment measurements

Particle alignment at 36.5 MHz is shown for dual-IDT operation in figure 6(*B*). Single-IDT operation also enabled alignment at 36.5 MHz, as shown in figure 6(*C*). The possibility of operation with only one transducer makes the total device smaller and extends the fluidic channel design possibilities. The alignment occurred into three nodes at the channel middle and the channel walls. For a speed of sound in water of 1500 m s^{-1}, the wavelength in water at 36.5 MHz is 41 μm; hence, the channel width encompasses approximately 1.5 λ, i.e. can display three pressure nodes. The particles were observed to align quickly in the channel to a narrow focus region estimated to 13% of the channel width, i.e. 7.5 μm. The small width of the nodal region of this system is advantageous for precise alignment of single cell and small bioparticles. The voltage levels and channel lengths employed are clearly adequate to accomplish the desired alignment effect at these flow velocities. The 1.8 μm diameter particle size is in the range of the minimum particle size usually employed for manipulation with BAW transducers (usually larger than 1 μm diameter polystyrene beads), i.e. the forces are at least on a comparable level. The voltage across the electrodes at the frequency of operation was 10 Vpp, as measured by an oscilloscope. Many factors are expected to influence the frequency of best operation, such as efficient coupling from the function generator, substrate geometry, channel size and geometry.

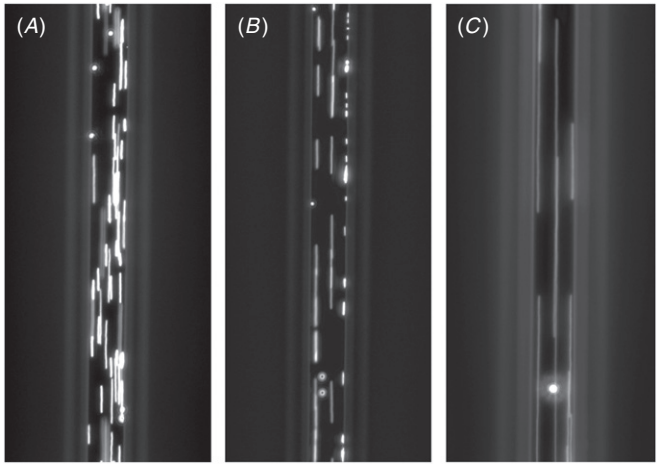

Figure 6. Particle alignment of the 1.9 μm polystyrene beads in the 60 μm wide trapezoidal channels for (*A*) transducer off, (*B*) single-IDT operation and (*C*) dual operation by the two IDTs in series. Close to the channel wall, the particles move more slowly due to the parabolic flow profile as observed by shorter brighter lines. In (*C*), the exposure time was longer and the image brightness was lower resulting in longer less bright lines as compared with (*B*). Some particles sticking to the channel walls appear as circular spots.

The observed symmetric node alignment relative to the channel walls supports the glass/fluid interface as the main origin of reflection rather than the outer boundaries of the glass structure since the channel is not expected to be perfectly aligned with the IDTs or the glass boundaries. For such a case, it can be envisaged that the shape of the channel wall, i.e the resonance cavity, is important and that optimizing its geometry can improve the manipulation performance.

No acoustic streaming, which could degrade the separation performance, was observed at continuous flow operation. Suppression of acoustic streaming is favored by low driving voltage, low frequency [66] and large particles [67] but is also affected by for instance the channel geometry [54].

No other frequencies were observed to generate alignment in the 0.1 MHz step-size frequency scan. It was not observed whether the alignment also occurred in the vertical direction.

The multi-node design, as an alternative, can be used for separation but requires a more complex fluidic outlet design, for instance, as is used for field flow fractionation [13]. If sheath flow is used on either side of the sample flow, the present design can also be used for single node alignment. Based on the geometric profile, the sheath:sample volume ratio would be approximately 0.8; hence, the proportion sheath:sample is 2.6 lower than for the system described by Grenvall *et al* [53]. For a certain volume flow rate, the amount of sheath volume needed is 100 times less (and the sample volume 30 times lower) since the operational frequencies and channel sizes are different.

4.3. FEM modeling of acoustic fields

FEM simulation results are shown in figure 7. A periodic pattern of a standing wave, a SSAW [18], is observed in the lithium niobate substrate, figure 7(*A*). The displacement amplitude in the substrate is observed to generate a pressure amplitude pattern in the glass superstrate which does not change with the plot angle and hence is standing. To some extent, the acoustic field in the superstrate can be regarded as excited by an amplitude-modulated line source at the substrate interface. The pressure amplitude in the glass superstrate displays maximum values along the boundary layer region and at the fluid cavity boundary. This localization to the interface region is advantageous for transporting energy efficiently to the fluid layer rather than transmitting a large amount to the surrounding glass structure. The fluidic cavity is smaller than the SAW wavelength and the cavity can be thought of as an inhomogeneity at the interface region. The wavelength in the glass layer, 155 μm at 36.5 MHz, is larger than the SAW wavelength.

Reflections at the glass superstrate outer boundaries are observed as expected since perfectly matched layers (PML) are not used in the simulation model but rather an outer absorbing glass layer. However, no strong resonance build up in the glass layer is observed and it is possible to use the model to mainly visualize effects related to the interface region and the fluid cavity. The positions of the maximum pressure amplitude in the superstrate do not perfectly correspond to the position of the maximum displacement amplitude in the substrate. This effect is believed to originate from the bonding layer since corresponding positions are observed in the simulation if the bonding layer is removed.

At 36.5 MHz, the acoustic radiation force potential for a 1.9 μm polystyrene particle in the fluid layer displays minima in a narrow region in the middle of the channel and at two small regions close to the channel walls, figure 7(*B*), in agreement with the measurements. The inter-node distance is less than the SAW half-wavelength. Hence, the inter-node distance observed here in the measurements and simulations is different from the λSSAW/2 inter-node distance most often reported for other SAW-transducer systems with the PDMS channel [18] or without side-walls [42]. At the center position, a displacement minima is found at the substrate and an acoustic radiation force potential minima for a polystyrene particle in the fluid layer, i.e. a pressure minima. The shape of the middle node is a line with absolute minima close to the bottom while the shapes of the side nodes are elliptical regions oriented parallel with the tapered channel walls. The nodal minima are located to small areas with the diameter of a couple of μm. The very precise alignment to a small spot is advantageous in many applications. However, for alignment of very large cells, there will be a non-zero net force on the outer regions of the cell in the acoustic gradient field also when it has been aligned to a node. The magnitude of the force depends on the cell size relative to the node size and the steepness of the acoustic gradient field. The position in the vertical direction close to the bottom fluid wall was not possible to verify in the experiment. Comparing the measurements and the simulation results, one finds that in the measurements the position of the side nodes appears to be closer to the side walls than in the simulations. The origin for the discrepancy is not understood at this point. Possibly, if some SU8 has been pushed into the channel, it can appear narrower and the alignment positions seem to be closer to the

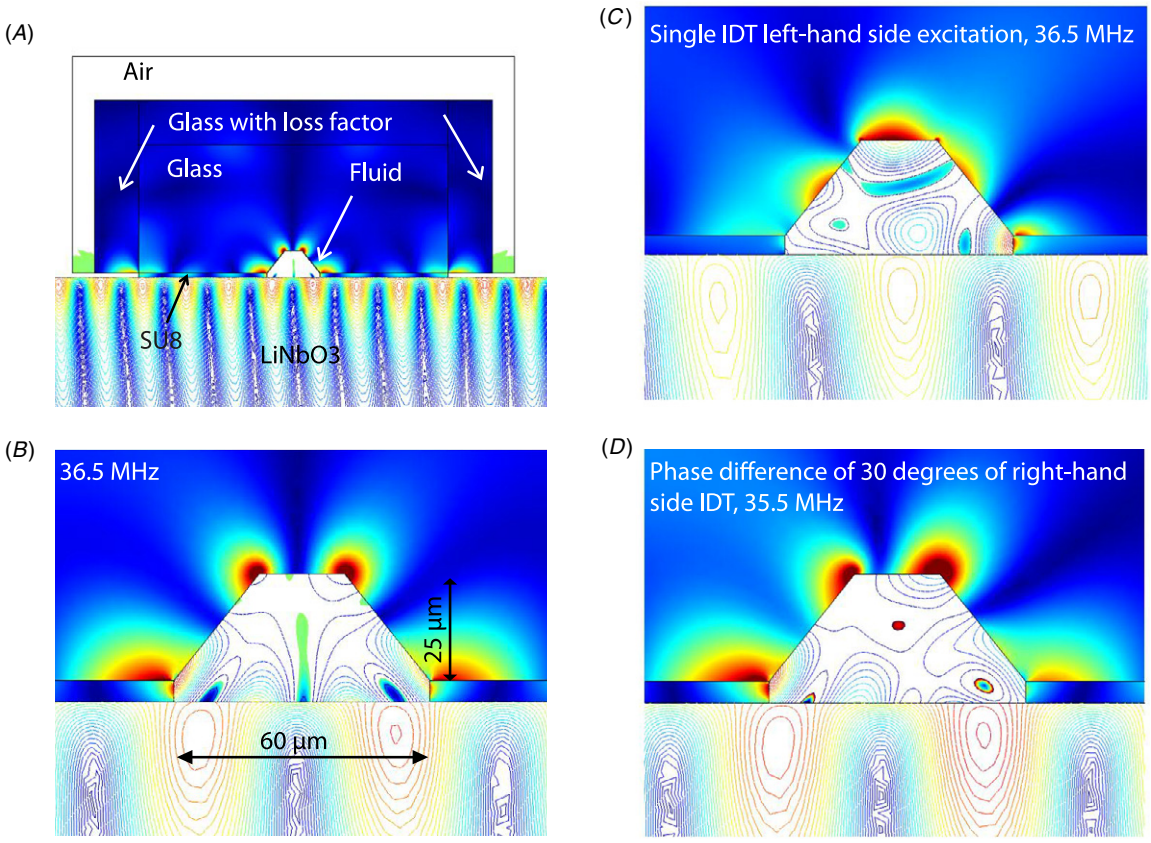

Figure 7. FEM-simulation results for the channel cross-section at 36.5 MHz for displacement amplitude in the piezoelectric material, pressure amplitude in the glass layers and the bond layer and acoustic radiation force potential in the fluidic layer for the 1.9 μm polystyrene particles (red color = maximum value, blue color = minimum value. In the $LiNbO_3$ layer the displacement amplitude minima are observed as narrow regions between the larger displacement maxima regions. In the glass layer the pressure amplitude maxima are found mainly at edges along the fluid cavity interface.) (*B*) Close-up of the fluid cavity. The appearance of the acoustic field for (*C*) excitation by single IDT from the left-hand side and (*D*) by two IDT operations with phase shift of 30° for the right-hand side IDT signal. The absolute values are low since only few IDT strips are modeled. Displacement amplitude is in the range of max 0.4 nm, pressure amplitude in the range of max 0.1 MPa and acoustic radiation force potential minima in the range of −2–40 aN.

channel walls. When changing the frequency in the range 35–37 MHz, the pattern does not change much. Hence, it can be expected that a small misalignment will not significantly alter the alignment positions in the channel. However, from the frequency sensitivity observed in the measurements, many factors are expected to significantly influence the magnitude of the field in the channel.

Based on the impedance mismatch at the cavity boundary, it is expected that the appearance of the acoustic radiation force potential in the fluid layer will be highly influenced by reflections inside the cavity. Hence, by proper system design, the glass channel geometry can be used as an additional parameter for shaping the acoustic field in the vertical direction. In support of this expectancy are the inter-node distances observed in measurements, the shape of the side nodes in the simulation and the insensitivity to frequency variation in the simulation.

For simulation with one IDT excitation, figure 7(*C*), three nodes were also observed and the inter-node distances and horizontal positions were approximately the same as for dual IDT excitation, i.e. corresponding to the measurement observations. However, in the simulation, the node pattern was not perfectly symmetric and the middle node was shifted upward and oriented horizontally instead of vertically. A similar horizontal alignment pattern for both single- and double-IDT operations supports the channel cavity as a major influence for the appearance of the acoustic field in the fluidic layer.

When altering the phase of one of the IDTs by 30°, figure 7(*D*), the shape of all three nodes are circular and the middle node is positioned higher up in the fluid layer away from the bottom surface. Same as in figure 7(*B*), the alignment into specific positions of small area is observed.

Considering the number of parameters that can potentially have an effect on the acoustic field in the fluid in addition to the poor alignment precision obtained in the manual alignment step makes system design appear to be very complex. However, several parameters such as driving frequency and phase can be tuned and the channel length is expected to have an averaging effect on misalignment effects such that a small region of non-ideal pattern can be acceptable. From simulation and measurement, some main factors influencing the operation were identified, such as energy localization to the interface region and the influence of channel size and geometry. Additionally, the outer structures of the channel are expected to influence the acoustic pattern, but

for the selected device geometry this effect appears to be smaller or in support of the same alignment pattern. It is expected that a system design optimum exists corresponding to a certain channel width, channel position and channel geometry. However, for these non-optimized devices, it is shown that the created acoustic field is strong enough to enable competitive manipulation performance with both dual and single excitations. Future work may extend applications of this type of systems to also include sheathless alignment into one single node for pre-alignment for sorting, detection and field flow fractionation.

5. Conclusions

A device for particle manipulation in continuous flow where a surface acoustic wave was used to excite an acoustic field in a trapezoidal glass channel has been demonstrated. This work extends the use of SAWs for acoustic manipulation in PDMS and the more exclusive material and design used for IAW to also include the microfluidic commonly used glass material. In a proof-of-principle measurement, the alignment of 1.9 μm polystyrene beads was demonstrated at 35.6 MHz into three pressure nodes symmetrically in a 60 μm wide trapezoidal channel. The precise alignment into small nodes makes the system interesting for manipulation and analysis of small cells or bioparticles. Similar to glass-channel-BAW transducer systems, the size and shape of the channel have strong influence on the appearance of the acoustic field in the channel. In contrast to previous SAW devices featuring PDMS channels, the inter-node distance here was shorter, in the range of $\lambda_{water}/2$.

From a FEM simulation model, some main factors influencing the operation were suggested, such as energy localization to the interface region and the influence of channel size and shape. In simulation, the simultaneous 2D alignment into small nodes positioned close to a surface or in the fluid layer was obtained for the operating frequency and dual or single IDT operation. Simultaneous vertical and 2D alignment by a single frequency is not commonly performed in microstructured channels by acoustic particle manipulation and has applications in alignment prior to sensor detection. However, additional measurements are needed to verify the vertical alignment positions predicted by the simulations. Future work may extend applications of this type of systems to also include 2D alignment into one single node without sheath flow for pre-alignment for sorting, detection and field flow fractionation in sheathless operation and parabolic flow profile. For these non-optimized devices, it is shown that the created acoustic field is strong enough to enable competitive manipulation performance with both dual and single IDT excitations.

Acknowledgments

We would like to acknowledge Professor Anders Rydberg at Signals and Systems Department Uppsala University for providing the function generator and Dr Zhigang Wu Material Science Uppsala University for providing the micro beads. Hanna Yousef is acknowledged for taking the SEM-images. SSF MS2E and Vinnex WISENET are acknowledged for financial support.

References

[1] Harris N R, Hill M, Beeby S, Shen Y, White N M, Hawkes J J and Coakley W T 2003 A silicon microfluidic ultrasonic separator *Sensors Actuators* B **95** 425–34

[2] Hawkes J J, Barber R W, Emerson D R and Coakley W T 2004 Continuous cell washing and mixing driven by an ultrasound standing wave within a microfluidic channel *Lab on a Chip* **4** 446–52

[3] Laurell T, Petersson F and Nilsson A 2007 Chip integrated strategies for acoustic separation and manipulation of cells and particles *Chem. Soc. Rev.* **36** 492–506

[4] Nield A, Oberti S, Radziwill G and Dual J 2007 Simultaneous positioning of cells into two-dimensional arrays using ultrasound *Biotechnol. Bioeng.* **97** 1335–9

[5] Coakley W T 1997 Ultrasonic separations in analytical biotechnology *Trends Biotechnol.* **15** 506–11

[6] Wiklund M, Gunther C, Lemor R, Jager M, Fuhr G and Hertz H M 2006 Ultrasonic standing wave manipulation technology integrated into a dielectrophoretic chip *Lab on a Chip* **6** 1537–44

[7] Oberti S, Neild A, Quach R and Dual J 2009 The use of acoustic radiation forces to position particles within fluid droplets *Ultrasonics* **49** 47–52

[8] Bazou D, Blain E J and Coakley W 2008 NCAM and PSA-NCAM dependent membrane spreading and F-Actin reorganization in suspended adhering neural cells *Mol. Membrane Biol.* **25** 102–14

[9] Evander M, Johansson L, Lilliehorn T, Piskur J, Lindvall M, Johansson S, Almqvist M, Laurell T and Nilsson J 2007 Noninvasive acoustic cell trapping in a microfluidic perfusion system for online bioassays *Anal. Chem.* **79** 2984–91

[10] Petersson F, Nilsson A, Jonsson H and Laurell T 2005 Carrier medium exchange through ultrasonic particle switching in microfluidic channels *Anal. Chem.* **77** 1216–21

[11] Augustsson P, Persson J, Ekstrom S, Ohlin M and Laurell T 2009 Decomplexing biofluids using microchip based acoustophoresis *Lab on a Chip* **9** 810–8

[12] Petersson F, Nilsson A, Holm C, Jonsson H and Laurell T 2004 Separation of lipids from blood utilizing ultrasonic standing waves in microfluidic channels *Analyst* **129** 938–43

[13] Petersson F, Aberg L, Sward-Nilsson A and Laurell T 2007 Free flow acoustophoresis and microfluidic-based mode of particle and cell separation *Anal. Chem.* **79** 5117–23

[14] Johansson L, Nikolajeff F, Johansson S and Thorslund S 2009 On-chip fluorescence activated cell sorting by an integrated miniaturized ultrasonic transducer *Anal. Chem.* **81** 5188–96

[15] Johansson L, Johansson S, Nikolajeff F and Thorslund S 2009 Effective mixing of laminar flows at a density interface by an integrated ultrasonic transducer *Lab on a Chip* **9** 297–304

[16] Goddard G R, Sanders C K, Martin J C, Kaduchak G and Graves S W 2007 Analytical performance of an ultrasonic particle focusing flow cytometer *Anal. Chem.* **79** 8740–6

[17] Goddard G and Kaduchak G 2005 Ultrasonic particle concentration in a line-driven cylindrical tube *J. Acoust. Soc. Am.* **117** 3440–7

[18] Shi J J, Mao X L, Ahmed D, Colletti A and Huang T J 2008 Focusing microparticles in a microfluidic channel with standing surface acoustic waves (SSAW) *Lab on a Chip* **8** 221–3

[19] Shi J J, Ahmed D, Mao X and Huang T J 2008 Surface acoustic wave (SAW) induced patterning of micro beads in

microfluidic channels *21st IEEE Int. Conf. on Micro Electro Mechanical Systems—MEMS '08* pp 26–9
[20] Nam J, Lee Y and Shin S 2011 Size-dependent microparticles separation through standing surface acoustic waves *Microfluid. Nanofluid.* **11** 317–26
[21] Yeo L Y and Friend J R 2009 Ultrafast microfluidics using surface acoustic waves *Biomicrofluidics* **3** 012002
[22] Wixforth A 2003 Acoustically driven planar microfluidics *Superlatt. Microstruct.* **33** 389–96
[23] Tan M K, Friend J R and Yeo L Y 2007 Microparticle collection and concentration via a miniature surface acoustic wave device *Lab on a Chip* **7** 618–25
[24] Shiokawa S, Matsui Y and Moriizumi T 1989 Experimental study on liquid streaming by SAW *Japan. J. Appl. Phys.* **28** 126–8
[25] Shiokawa S, Matsui Y and Ueda T 1990 Study on SAW streaming and its application to fluid devices *Japan. J. Appl. Phys.* **29** 137–9
[26] Kurosawa M, Watanabe T, Futami A and Higutchi T 1995 Surface acoustic wave atomizer *Sensors Actuators* **50** 69–74
[27] Li H, Friend J R and Yeo L Y 2008 Microfluidic colloidal island formation and erasure induced by surface acoustic wave radiation *Phys. Rev. Lett.* **101** 084502
[28] Sritharan K, Strobl C J, Schneider M F and Wixforth A 2006 Acoustic mixing at low Reynold's numbers *Appl. Phys. Lett.* **88** 054102
[29] Tseng W-K, Lin J-L, Sung W-C, Chen S-H and Lee G-B 2006 Active micro-mixers using surface acoustic waves on Y-cut 128° $LiNbO_3$ *J. Micromech. Microeng.* **16** 539–48
[30] Lindner G, Faustmann H, Fischer T, Krempel S, Münch M, Rothballer S and Schmitt M 2007 Acoustic surface wave induced propagation of liquids in open channels *Proc. IEEE Ultrason. Symp.* pp 2331–4
[31] Cecchini M, Girardo S, Pisignano D, Cingolani R and Beltram F 2008 Acoustic-counterflow microfluidics by surface acoustic waves *Appl. Phys. Lett.* **92** 104103
[32] Franke T, Abate A R, Weitz D A and Wixforth A 2009 Surface acoustic wave (SAW) directed droplet flow in microfluidics for PDMS devices *Lab on a Chip* **9** 2625–7
[33] Tan M K, Tjeung R, Ervin H, Yeo L Y and Friend J 2009 Double aperture focusing transducer for controlling microparticle motions in trapezoidal microchannels with surface acoustic waves *Appl. Phys. Lett.* **95** 134101
[34] Yantchev V, Enlund J, Katardjiev I and Johansson L 2010 A micromachined Stoneley acoustic wave system for continuous flow particle manipulation in microfluidic channels *J. Micromech. Microeng.* **20** 035031
[35] Mukhopadhyay R 2009 Hard-soft microfluidic device bypasses drawbacks of PDMS *Anal. Chem.* **81** 4169–73
[36] Shin Y S, Cho K, Lim S H, Chung S, Park S-J, Chung C, Han D-C and Chang J K 2003 PDMS-based micro PCR chip with parylene coating *J. Micromech. Microeng.* **13** 768–74
[37] Huang B, Wu S, Andl Kim H and Zare R N 2005 Coating of poly(dimethylsiloxane) with *N*-Dodecyl-β-D-Maltoside to minimize nonspecific protein adsorption *Lab on a Chip* **5** 1005–7
[38] Wu K and Ang Hjort Z 2009 Surface modification of PDMS by gradient-induced migration of embedded Pluronic *Lab on a Chip* **9** 1500–3
[39] Xiao Y, Yu X-D, Xu J-J and Chen H-Y 2007 Bulk modification of PDMS microchips by an amphiphilic copolymer *Electrophoresis* **28** 3302–7
[40] Lee J N, Park C and Whitesides G 2003 Solvent compatibility of poly(dimethylsiloxane)-based microfluidic devices *Anal. Chem.* **75** 6544–54
[41] Huikko K *et al* 2003 Poly(dimethylsiloxane) electrospray devices fabricated with diamond-like carbon-poly(dimethylsiloxane) coated SU-8 Masters *Lab on a Chip* **3** 67–72
[42] Wood C D, Evans S D, Cunningham J E, O'Rorke R, Walti C and Davies A G 2008 Alignment of particles in microfluidic systems using standing surface acoustic waves *Appl. Phys. Lett.* **92** 044104
[43] Manneberg O, Svennebring J, Hertz H M and Wiklund M 2008 Wedge transducer design for two-dimensional ultrasonic manipulation in a microfluidic chip *J. Micromech. Microeng.* **18** 095025
[44] Manneberg O, Vanherberghen B, Svennebring J, Hertz H M, Onfelt B and Wiklund M 2008 A three-dimensional ultrasonic cage for characterization of individual cells *Appl. Phys. Lett.* **93** 063901
[45] Manneberg O, Hagsater S M, Svennebring J, Hertz H M, Kutter J P, Bruus H and Wiklund M 2009 Spatial confinement of ultrasonic force fields in microfluidic channels *Ultrasonics* **49** 112–9
[46] Evander M, Lenshof A, Laurell T and Nilsson J 2008 Acoustophoresis in wet-etched glass chips *Anal. Chem.* **80** 5178–85
[47] Hill M, Townsend R J and Harris N R 2008 Modelling for the robust design of layered resonators for ultrasonic particle manipulation *Ultrasonics* **48** 521–8
[48] Hill M, Hawkes J J, Harris N R and McDonnel M B 2004 Resonant ultrasonic particle manipulators and their applications in sensor systems *Proc. IEEE Sensors 2004 (Vienna, 24–27 October 2004)* vols 1–3 ed D Rocha, P M Sarro and M J Vellekoop pp 794–7
[49] Townsend R J, Hill M, Harris N R and McDonnell M B 2008 Performance of a quarter-wavelength particle concentrator *Ultrasonics* **48** 515–20
[50] Glynne-Jones P, Boltryk R J, Hill M, Zhang F, Dong L, Wilkinson J S, Melvin T, Harris N R and Brown T 2009 Flexible acoustic particle manipulation device with integrated optical waveguide for enhanced microbead assays *Anal. Sci.* **25** 285–91
[51] Glynne-Jones P, Boltryk R J, Hill M, Harris N R and Baclet P 2009 Robust acoustic particle manipulation: a thin-reflector design for moving particles to a surface *J. Acoust. Soc. Am.* **126** EL75–9
[52] Glynne-Jones P, Boltryk R J, Harris N R, Cranny A W J and Hill M 2010 Mode switching: a new technique for electronically varying the agglomeration position in an acoustic particle manipulator *Ultrasonics* **50** 68–75
[53] Grenvall C, Carlsson M, Augustsson P, Petersson F and Laurell T 2007 Fluorescent activated cell sorter using ultrasound standing waves in micro channels *Proc. Micro Total Analysis Systems μTAS2007* pp 1813–5
[54] Sobanski M A and Coakley T X 2001 Sub-micron particle manipulation in an ultrasonic standing wave: applications in detection of chemically important biomolecules *Bioseparation* **9** 351–7
[55] Shi J, Yazdi S-C S, Lin S, Ding X, Chiang I-K, Sharp K and Huang T J 2011 Three-dimensional continuous particle focusing in a microfluidic channel via standing surface acoustic waves (SSAW) *Lab on a Chip* **11** 2319–24
[56] Wiklund M, Toivonen J, Tirri M, Hanninen P and Hertz H M 2004 Ultrasonic enrichment of microspheres for ultrasensitive biomedical analysis in confocal laser-scanning fluorescence detection *J. Appl. Phys.* **96** 1242–8
[57] Wiklund M and Hertz H M 2006 Ultrasonic enhancement of bead-based bioaffinity assays *Lab on a Chip* **6** 1279–92
[58] Jyomura S, Nagatsuma K and Takeuchi H 1981 SAW propagation loss mechanism in piezoelectric ceramics *J. Appl. Phys.* **52** 4472–8
[59] Kinsler L E, Frey A R, Coppens A B and Sanders J V 2000 *Fundamentals of Acoustic* 4th edn (New York: Wiley)

[60] Zell K, Sperl J I, Vogel M W, Niessner R and Haisch C 2007 Acoustical properties of selected tissue phantom materials for ultrasound imaging *Phys. Med. Biol.* **52** N475–84
[61] Wiemer M, Jai C, Toepper M and Hauck K 2006 Wafer bonding with BCB and SU8 for MEMS packaging *IEEE Electronics System Integration Technology Conf.* pp 1401–5
[62] Iliescu C, Tay F and Miao J 2007 Deep wet etching through 1 mm pyrex glass wafer for microfluidic applications *Sensors Actuators* A **133** 395–400
[63] Kal S, Haldar S and Lahiri S K 1990 Slope etching of silicon dioxide *Microelectron. Reliab.* **30** 719–22
[64] Majjad H, Gachon D, Laude V and Ballandras S 2006 Interface acoustic wave devices made by indirect bonding of lithium niobate on silicon *2006 IEEE Ultrasonic Symp.* pp 1193–6
[65] Gachon D, Majad H, Daniau W, Laude V and Ballandras S 2007 Excitation of acoustic waves at the interface between lithium niobate and silicon plates *Int. Frequency Control Symp. 2007 Joint With the 21st European Frequency and Time Forum IEEE* pp 733–6
[66] Rozenberg L 1971 *High Intensity Ultrasonic Fields* (New York: Plenum)
[67] Spengler J F, Coakley W T and Christensen K T 2003 Microstreaming effects on particle concentration in an ultrasonic standing wave *AIChE J.* **49** 2773–82